J. Fluid Mech. (2002), *vol.* 467, *pp.* 19–40.
DOI: 10.1017/S0022112002001350 Printed in the United Kingdom

Turbulent thermal convection in a rotating stratified fluid

By M. A. LEVY AND H. J. S. FERNANDO

Environmental Fluid Dynamics Program, Department of Mechanical and Aerospace Engineering, Arizona State University, Tempe, AZ 85287-9809, USA

(Received 8 December 1998 and in revised form 10 March 2002)

Turbulent convection induced by heating the bottom boundary of a horizontally homogeneous, linearly (temperature) stratified, rotating fluid layer is studied using a series of laboratory experiments. It is shown that the growth of the convective mixed layer is dynamically affected by background rotation (or Coriolis forces) when the parameter $R = (h^2\Omega^3/q_0)^{2/3}$ exceeds a critical value of $R_c \approx 275$. Here h is the depth of the convective layer, Ω is the rate of rotation, and q_0 is the buoyancy flux at the bottom boundary. At larger R, the buoyancy gradient in the mixed layer appears to scale as $(\mathrm{d}\bar{b}/\mathrm{d}z)_{ml} = C\Omega^2$, where $C \approx 0.02$. Conversely, when $R < R_c$, the buoyancy gradient is independent of Ω and approaches that of the non-rotating case. The entrainment velocity, u_e, for $R > R_c$ was found to be dependent on Ω according to $E = [Ri(1 + C\Omega^2/N^2)]^{-1}$, where E is the entrainment coefficient based on the convective velocity $w_\star = (q_0 h)^{1/3}$, $E = u_e/w_\star$, Ri is the Richardson number $Ri = N^2h^2/w_\star^2$, and N is the buoyancy frequency of the overlying stratified layer. The results indicate that entrainment in this case is dominated by non-penetrative convection, although the convective plumes can penetrate the interface in the form of lenticular protrusions.

1. Introduction

Turbulent thermal convection is common in geophysical and engineering flows. Examples include the daytime convective boundary layer in the atmosphere, convection in the upper ocean due to nocturnal cooling and deep-ocean convection. One of the simplest cases of turbulent convective flow occurs when a fluid layer between two parallel plates, separated by a distance h, is subjected to an unstable temperature difference of ΔT. If the thermal diffusivity of the fluid is κ and the kinematic viscosity is ν, then the nature of turbulent convection is dependent on the Rayleigh number Ra and Prandtl number Pr, defined as (Turner 1973)

$$Ra = \frac{g\alpha\Delta T h^3}{\kappa\nu} \quad \text{and} \quad Pr = \frac{\nu}{\kappa}, \tag{1.1}$$

where g is the gravitational acceleration and α is the thermal expansivity. Krishnamurty (1970) has mapped different regimes that appear in this type of turbulent convection on a (Ra, Pr)-plane, which shows that turbulent convection is possible when $Ra > 1.4 \times 10^4 Pr^n$, where $n \approx 1.4$ for $Pr < 20$. A related, but more geophysically relevant, case is convection between two parallel plates driven by a bottom heat flux Q_0, or equivalently a buoyancy flux $q_0 = g\alpha Q_0/\rho_0 c_p$, where ρ_0 is a reference density and c_p is the specific heat at constant pressure. In this case, the governing

parameters are the Prandtl number and the flux Rayleigh number Ra_f, defined as

$$Ra_f = \frac{q_0 h^4}{\kappa^2 \nu}. \tag{1.2}$$

Willis & Deardorff (1974) argued that turbulent convection occurs when $Ra_f > 10^5$ or so. Numerical simulations on the planetary boundary layer by Deardorff (1972) show that in pure turbulent convection (i.e. away from the surface layer and other boundary layers where shear is dominant) the r.m.s. horizontal u and vertical w velocities and the length scale L can be given by

$$L = C_1 h, \tag{1.3a}$$

$$u = C_2 w_\star, \tag{1.3b}$$

and

$$w \sim u, \tag{1.3c}$$

where C_1 and C_2 are constants, and the convective velocity $w_\star$ is defined as

$$w_\star = (q_0 h)^{1/3}. \tag{1.4}$$

Since no shear is present in our study, the velocity and length scales of convection in the central portion of the layer are expected to follow (1.3). At high Ra_f, convection is strong enough that the molecular parameters do not play a governing role away from the boundaries. The forms (1.3*a–c*) have been verified by numerous laboratory and numerical experiments (Deardorff & Willis 1985; Adrian, Ferreira & Boberg 1986; Jones & Marshall 1993; Molemaker & Dijkstra 1997), and field observations (Kaimal *et al.* 1976). Extensive reviews on this subject are given in Adrian *et al.* (1986), Castaing *et al.* (1989), and Siggia (1994).

Although the problem of convection between two parallel plates is a useful first step, convection in geophysical flows has many dynamical complications, moving boundaries and the influence of Earth's rotational effects, to name two. The effects of background rotation have been investigated by numerous workers focusing on the rich variety of flow phenomena that occur when the governing parameters are varied (Boubnov & Golitsyn 1995; Fernando & Smith 2001). Rotation introduces an additional non-dimensional number to the problem, namely, the Taylor number defined as

$$Ta = \frac{4\Omega^2 h^4}{\nu^2}, \tag{1.5}$$

where Ω is the angular speed of rotation. The case of rotating turbulent convection in horizontally homogeneous fluid layers has been considered by Fernando, Chen & Boyer (1991), who provided experimental evidence to support that the r.m.s. velocity and integral length scales (with subscript r denoting the presence of rotation) are given by

$$w_r \sim u_r \approx 1.7 \left(\frac{q_0}{\Omega}\right)^{1/2}, \tag{1.6a}$$

and

$$L_r \approx 1.1 \left(\frac{q_0}{\Omega^3}\right)^{1/2}, \tag{1.6b}$$

with rotation playing an important role in constraining the growth of turbulent scales in directions perpendicular to the axis of rotation. They also showed that the rotational effects become important when the turbulent Rossby number $Ro = u/2\Omega L$

becomes smaller than about 0.75, although, according to Fluery *et al.* (1991), the Rossby number must drop into the range of 0.2–0.36 before turbulence becomes quasi-two-dimensional. Applications of this result to atmospheric and some oceanic flows reveal that the properties of convective turbulence in such flows are hardly affected by background rotation, except for large-scale convective flows and/or at smaller buoyancy fluxes. Numerical simulation studies (Julien *et al.* 1996, 1999), however, indicate that certain features of the flow can be affected drastically by the presence of rotation even though the turbulent motions might not have felt the rotational effects. For example, near the horizontal boundaries delivering the buoyancy flux, the flow can be affected by the Ekman layers that dissipate significant amounts of kinetic energy and the breakdown of the thermal boundary layer near the surface may produce intermittently appearing ephemeral cyclonic vortices that protrude into the convective layer (Chen, Fernando & Boyer 1989).

The next level of complexity that can be imposed on rotating Rayleigh–Bénard convection is the presence of slowly moving boundaries. A geophysically relevant example of this case is the penetrative convection, wherein the convective layer is bounded by a stably stratified layer. Here the entrainment is taking place by the action of turbulent eddies engulfing fluid from the interfacial layer that separates the turbulent and non-turbulent layers (entrainment interface), overcoming the interfacial buoyancy jump $\Delta b \neq 0$ across these layers. The evolution of heat-stratified non-rotating fluids subjected to bottom heating has been the subject of numerous laboratory investigations, which trace back to the work of Deardorff, Willis & Lilly (1969). In these studies, the initial mean temperature ($\overline{T}$) stratification was specified by the buoyancy frequency $N^2 = -(g/\rho_0)\mathrm{d}\bar{\rho}/\mathrm{d}z = \mathrm{d}\bar{b}/\mathrm{d}z$, where $\bar{\rho}$ is the mean density, z is the vertical coordinate, $\bar{b}$ is the mean buoyancy, and the time evolution of flow upon imposition of a buoyancy flux q_0 was studied; see figure 1(*a*) for the initial flow configuration at $t = 0$ and figure 1(*b*) for the evolving flow at $t = t$. Here the buoyancy b is defined in terms of the density ρ as $b = -g(\rho - \rho_0)/\rho_0$. In general, laboratory experiments performed with heat-stratified fluids have shown that the convective mixed layer evolves in such a way that $\Delta b \approx 0$ (Deardorff *et al.* 1969), implying that the convection is non-penetrative. Measurements taken during oceanic (Leaman & Schott 1991) and atmospheric (Kaimal *et al.* 1976) convection also have shown similar non-penetrative behaviour although there can be cases where the entrainment is penetrative (Sullivan *et al.* 1998).

In spite of the extensive work that has been carried out on convection in stratified non-rotating fluids, to our knowledge there is no laboratory experimental work reported on the effects of rotation on the growth of a horizontally homogeneous mixed layer in stratified fluids. There have been several experiments on convection induced by patches of unstable buoyancy sources discharging into linearly stratified rotating fluids to mimic oceanic deep convection, but the mixed-layer evolution in such cases is much different from the horizontally homogeneous convection in that the lateral baroclinic processes become important much quicker than the onset of rotational influence on turbulent entrainment (Ivey, Taylor & Coates 1995; Whitehead, Marshall & Hufford 1996; Colomer, Zieren & Fernando 1998). To our knowledge, this paper reports the first laboratory experimental study on the growth of a horizontally homogeneous convective mixed layer in a rotating linearly stratified fluid.

The present work was motivated by its possible application to the understanding of fluid dynamical phenomena related to deep ocean convection, which is characterized by turbulent convection in oceanic patches of horizontal extent of 10–100 km to depths of order 1–2 km. Convection driven by surface cooling is a common phenomenon

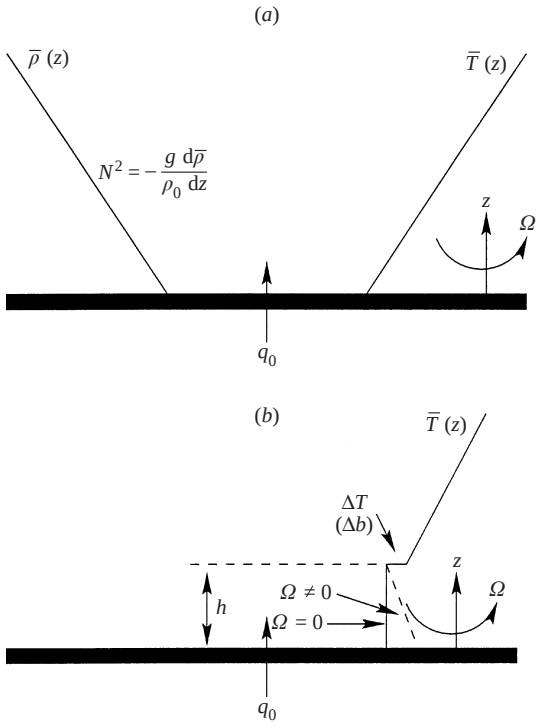

FIGURE 1. A schematic of turbulent thermal convection in a heat-stratified fluid subject to background rotation. (*a*) The initial mean temperature $\overline{T}(z)$ and mean density $\bar{\rho}(z)$ profiles at $t = 0$; (*b*) The temperature profile some time after the evolution of the bottom convective layer of thickness h. Note that the convective layer is topped by a density interface across which the buoyancy jump is Δb. The unstable molecular layers that develop near the bottom boundary are not shown for clarity.

in high-latitude oceans, but the typical depth of convection is constrained by the presence of a thermocline located at a depth on the order of 100 m. The deep convective regions are special, in that the thermocline is first domed upward by a preconditioning mechanism, thus forming an almost uniformly stratified layer near the surface. Then the stratification is eroded effectively by cooling-induced convection to produce a thick mixed water column with intense convection (Marshall & Schott 1998). In the laboratory, this process is modelled by releasing a plume of dense water onto a surface patch of rotating, linearly stratified fluid (Whitehead *et al.* 1996). Such experiments illustrate how the mixed layer initially propagates in a one-dimensional manner and lateral baroclinic eddy shedding becomes important thereafter. Although oceanic situations are aptly mimicked, the study of certain fundamental aspects of rotating convection is difficult in those experiments because of the dominance of several intermingled vertical and lateral processes in the convective layer. In the present study, a flow configuration that entails horizontal homogeneity of turbulence was selected to avoid the lateral processes so that the direct influence of rotation on the convective layer and its growth can be studied. It will be shown that background rotation leads to a dynamically important buoyancy gradient in the turbulent layer and the magnitude of this buoyancy gradient determines the growth rate of the mixed layer. Various criteria developed in the paper will be of utility in oceanic deep

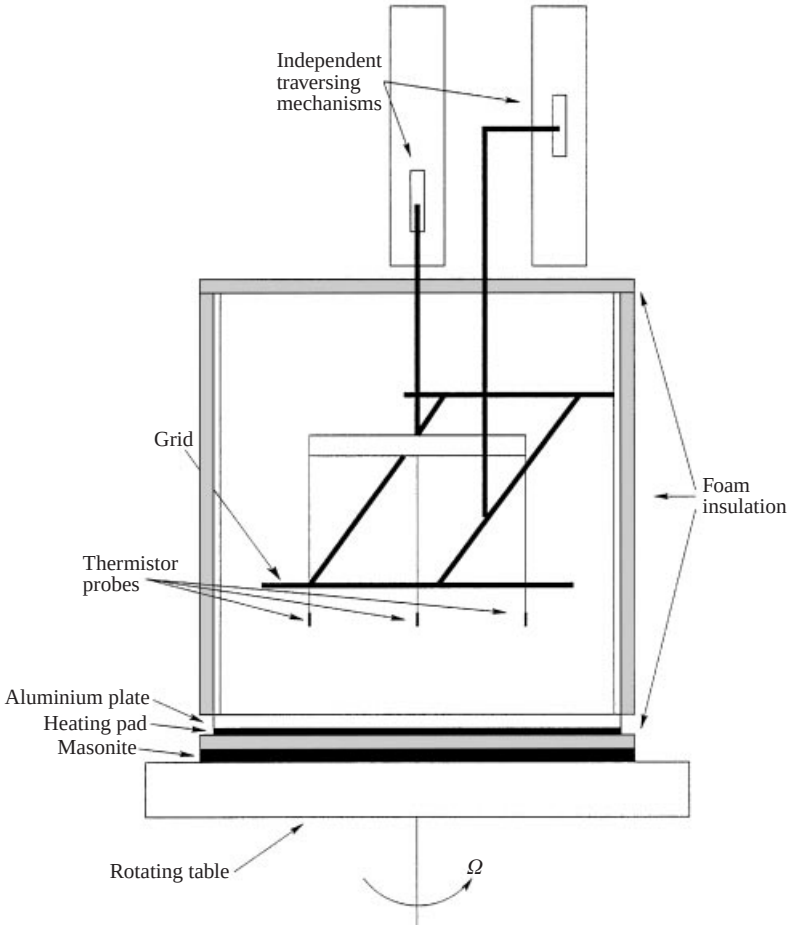

FIGURE 2. Schematic of experimental facility consisting of a 1.25 cm thick Plexiglas tank of dimensions $60 \times 60 \times 60$ cm. The heat is applied through a bottom aluminium plate of 1 cm thickness.

convection studies, although the generic experimental configuration considered here does not directly mimic deep convective situations.

The paper is organized as follows: In § 2, the experiments and measurement procedure are described. Some theoretical considerations pertinent to the problem are described in § 3. Experimental observations are described in § 4, which are used to identify the conditions under which rotational influence plays a dominant role and compare with the theoretical predictions of mixed-layer growth. A summary of salient results of this study together with their geophysical implications is given in § 5.

2. Experimental procedure

The experiments were conducted in a Plexiglas tank of dimensions $60 \times 60 \times 60$ cm, fitted with an aluminium bottom (1 cm thick) as shown in figure 2. This is the same tank and insulation used by Fernando *et al.* (1991). Below the metallic bottom was a layer of fibrous material, underneath which lay a custom-made heating pad, the heat output of which could be controlled via a variable-voltage power supply.

The heating pad and the sides of the pad/aluminium tank bottom assembly were insulated with polystyrene foam so that most of the heat generated at the heating pad flowed into the tank, evenly distributed across the bottom due to the fibrous material sandwiched in between. The tank sides were also covered with foil-faced polystyrene foam insulating sheets of thickness 3.75 cm, except during the short periods where side-view photographs were taken. The entire assembly was mounted on a rotating table capable of turning at angular velocities in the range $0.05 < \Omega < 1.5\,\mathrm{rad\,s^{-1}}$.

Fixed to the rotating platform was an instrument carriage and a traversing grid mechanism, which could be operated independently. The instrument carriage was fitted with a rake of three thermistor probes that could be traversed vertically into the stratified layer. One probe was centred in the tank, and the remaining two probes were located 15.2 cm in either direction from the centre probe along an axis parallel to the sidewalls. During their traverse, the probes recorded their temperature and location with a vertical step resolution of ± 1.0 mm. The measurement accuracy of the thermistor probes (response time of 7 ms) was estimated to be 0.1 °C based on the overall accuracy of the thermistors and A/D system. Temperature profiles were taken every 15 s at a platform traversing speed of $10\,\mathrm{cm\,s^{-1}}$. The data were read only during the downward traverse of the probes to prevent taking measurements in their own wakes. In some experiments, fluorescent dye was injected into the bottom convecting layer to visualize the flow structures. A 0.5 cm thick vertical sheet of light from a mercury lamp was shone through the centre of the tank parallel to the sidewall, and video recordings of dye patterns were made from the sides upon removal of the insulation.

The data acquisition and motion control of traverses were automated and were performed using a hardware package consisting of DAS-8/PGA, DAS-16 and EXP-GP data acquisition and signal monitoring boards (Metrabyte) as well as two (slo-syn 430-T) motor controllers. One controller was connected to a stepper motor driving the thermistor carriage through DAS-8/PGA, and the other was connected to the grid driving motor through DAS-16. The traverse position as well as thermistor output were fed into an EXP-GP signal conditioning system that provided multiplexing capabilities for simultaneous storage of digital data in a PC. The software for this automated system was developed in house and is given in Levy (1998). All hardware and computers were fixed to the rotating table, thus avoiding the problem of data transfer through slip rings.

The computer-controlled traversing grid mechanism was used to produce the initial linear stratification. A grid of overall dimensions 50×50 cm was made of 1.2 cm square Plexiglas rods with mesh size 5×5 cm. This was connected to a single rod, driven by a second traversing mechanism. The tank was initially filled with a layer of cold (5–25 °C) water underlying a layer of warm (30–55 °C) water, both layers having equal thicknesses, to produce a two-layer configuration with a total depth of 40 cm. The rotation of the system and the traversing grid mechanism were then both started, and several (3–5) grid traverses were made. Owing to the systematic vertical mixing resulting from the grid traverses through these fluid layers, a satisfactory linearly stratified fluid column was developed within the rotating tank, except near the top surface where evaporation and heat rejection to the ambient air caused the development of a mixed region. The fluid system was allowed to spin up for several hours to ensure solid body rotation, during which time all grid-induced motions also subsided. Figure 3(*a*) shows a typical initial mean temperature profile obtained by this technique by averaging 36 profiles. Then the heating of the stratified layer from the bottom was begun by switching on power to the heating coils. After several minutes,

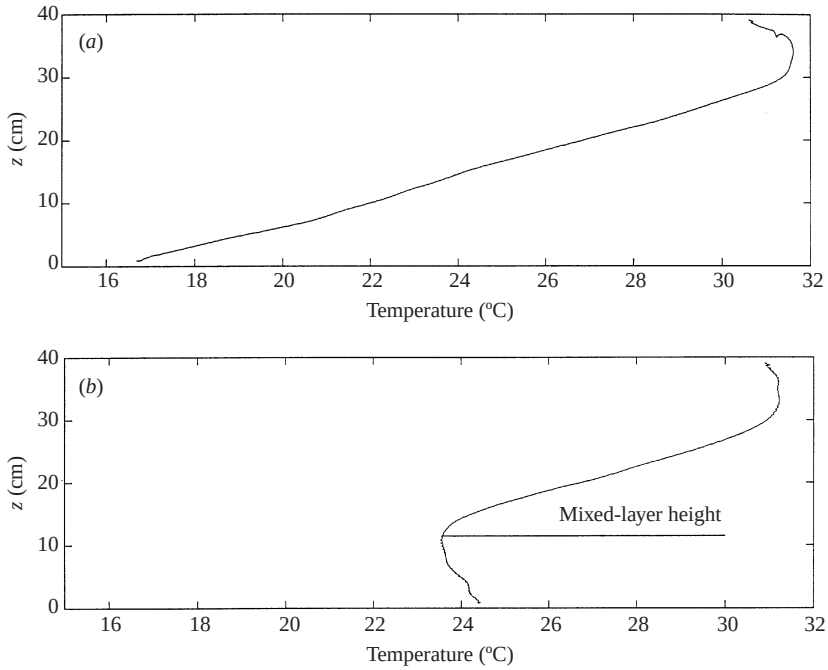

FIGURE 3. (*a*) A typical averaged temperature profile taken just before the heat flux is turned on. (*b*) A typical profile through the growing convective layer of $\Omega = 1.05\,\mathrm{rad\,s^{-1}}$, $q_0 = 0.02\,\mathrm{cm^2\,s^{-3}}$, $N^2 \approx 0.08\,\mathrm{s^{-2}}$.

the thermal (molecular) boundary layer that developed near the tank bottom broke down, thus producing a convectively mixed layer that grows with time. The growth of the mixed layer as a function of time was captured by recording temperature profiles. The mean temperature profiles were obtained by averaging a suitable number of temperature profiles (typically 6–48 depending on the entrainment velocity) and then low-pass filtering to remove any high-frequency fluctuations.

Prior to the stratified experiments, the heating pad was calibrated by filling the tank to a depth of 10 cm (fluid mass m) and measuring the rate of mean temperature ($\overline{T}$) rise of the homogeneous layer for different power settings. The heat flux to the water layer was calculated as $Q = (mc_p \mathrm{d}\overline{T}/\mathrm{d}t)A_b^{-1}$, where A_b is the plan cross-sectional area of the tank. Heat losses through the insulated sides and the top Q_L were properly accounted for in the calculation of heat input from the heating pads using standard techniques (see Voropayev & Fernando 1999). The total heat flux $Q_0 = Q + Q_L$ so evaluated was used to evaluate the buoyancy flux using the usual formula $q_0 = g\alpha Q_0/\rho_0 c_p$.

At the beginning of stratified experiments, the temperature profile was measured and the corresponding buoyancy frequency was calculated using

$$N^2 = g\alpha \frac{\mathrm{d}\overline{T}}{\mathrm{d}z}. \tag{2.1}$$

The N, Ω and q_0 values used are listed in table 1. During the experiments, the temperature profiles were recorded as the mixed layer grew with time. In calculating the mixed-layer height h, an averaged temperature profile was calculated using individual temperature profiles taken by the thermistors. Isopycnals in rotating fluids tend to curve, which might introduce errors in the measurement of mixed-layer depth using

Ω (rad s^{-1})	N^2 (rad^2 s^{-2})	q_0 (cm^2 s^{-3})
0.000	0.090	0.010
0.000	0.060	0.020
0.103	0.064	0.020
0.103	0.043	0.040
1.050	0.080	0.020
0.403	0.118	0.020
0.105	0.122	0.020
0.974	0.083	0.020
0.940	0.080	0.014
1.050	0.072	0.040
0.051	0.093	0.020
1.300	0.044	0.020
1.300	0.051	0.020
0.209	0.088	0.020
0.209	0.088	0.020
1.050	0.149	0.004
1.300	0.075	0.020
1.300	0.021	0.020
1.310	0.083	0.040
1.310	0.042	0.020
1.300	0.120	0.020
1.300	0.123	0.020
1.300	0.093	0.020
1.300	0.123	0.040
1.050	0.080	0.008

TABLE 1. Experimental conditions for stratified and rotating experiments.

temperature profiles. However, as discussed by Greenspan (1980), this curvature of isopycnals for the no-motion axisymmetric case can be neglected when $z/r > \Omega^2 r/2g$, where r is the radius. Assuming that this provides a useful estimate for the present case, it is possible to calculate $\Omega^2 r/2g \approx 0.017$ and $z/r \approx 0.66$ for a typical case of $\Omega \approx 1.5\,\mathrm{rad\,s^{-1}}$, $r \approx 15\,\mathrm{cm}$, $z \approx 10\,\mathrm{cm}$. Thus, the effects of isopycnal curvature on mixed-layer height measurements could be neglected.

The criterion based on mean temperature profiles employed by Julien *et al.* (1996) was used for the measurement of h. In this method, starting at a chosen point of the stratified layer, the temperature gradient was calculated at each point, progressing downward until the temperature gradient was less than 10% of the temperature gradient in the stratified region. The corresponding location was used to define the convective-layer height h. Experiments were conducted for different N and q_0 (specified by the power setting of the heating coils), and rotation rate Ω. Recognizing that q_0 for a given setting obtained during calibration runs can be different from that of stratified rotating experiments, the heat flux for the latter was independently evaluated by calculating the heat content of the temperature profiles taken at different times of the experiment. The techniques used to obtain heat losses were the same as those for calibration runs. The q_0 evaluated using the two techniques agreed within $\pm 9\%$ (which was the maximum deviation). Therefore, in subsequent calculations, q_0 obtained using the calibration runs was used.

Another important parameter of the present flow configuration is the buoyancy gradient in the mixed layer $(\mathrm{d}\bar{b}/\mathrm{d}z)_{ml}$. In calculating this quantity, $\overline{T}(z)$ data in the range $0.25 < z/h < 0.75$ were fitted with a straight line and the resulting temperature

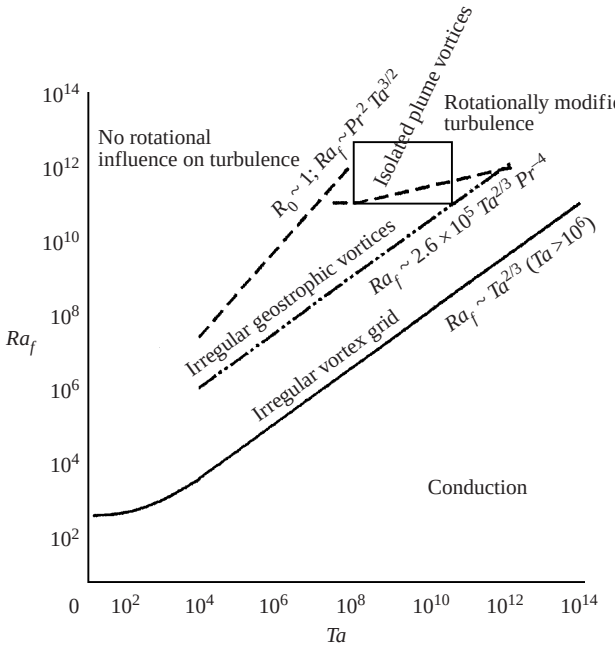

FIGURE 4. A composite regime diagram indicating possible flow regimes in rotating convection, based on examination of several previous studies, taken from Boubnov & Golitsyn (1995), where the nature of various rotating convection regimes is discussed in detail. The square box corresponds to the parameter regime used in the present study.

gradient was converted as $(\mathrm{d}\bar{b}/\mathrm{d}z)_{ml} = (g\alpha\,\mathrm{d}\overline{T}/\mathrm{d}z)$. The above bounds of z/h are expected to preclude the effects of the temperature boundary layer near the heating surface and the strong temperature fluctuations due to entrainment at the upper boundary. A typical temperature profile taken through a rotating convective boundary layer is shown in figure 3(b). During the investigation of the buoyancy gradient within the turbulent convective layer, several rotating experiments were also conducted with homogeneous water with an upper free surface as in Fernando *et al.* (1991). The evaluation of temperature gradients in these experiments was also the same as above. These experiments allowed expanded parameter ranges and systematic investigations of the onset of buoyancy gradients in the turbulent convective layer. As pointed out by Boubnov & Golitsyn (1995), the structure of rotating convection depends on the Ra_f and Ta used. The paramenter range used in the present study is shown in figure 4, where various flow patterns observed in rotating convection are illustrated based on Boubnov & Golitsyn (1995) and Fernando & Smith (2001). This diagram indicates that the flow in the present experiments is far from the marginal stability curve and is in the rotationally modified turbulence regime.

3. Theoretical considerations

As stated in § 1, there have been a number of laboratory experiments dealing with heating a stable temperature gradient from below in the absence of background rotation. In general, these experiments have indicated that the buoyancy gradient within the mixed layer is insignificantly small, and the convective layer can be considered as well mixed (figure 1b). Fernando *et al.* (1991) argued that this buoyancy

gradient $(\mathrm{d}\bar{b}/\mathrm{d}z)_{ml}$ should scale as

$$\left|\left(\frac{\mathrm{d}\bar{b}}{\mathrm{d}z}\right)_{ml}\right| \sim \frac{b'}{L} \sim \left(\frac{q_0}{w_\star}\right)\frac{1}{h} \sim \left(\frac{q_0}{h^2}\right)^{2/3}. \tag{3.1}$$

They pointed out, however, that in the presence of rotation ($\Omega \neq 0$) the vertical motions are impeded through Taylor–Proudman-type constraints and hence heavier water can be sustained over the lighter water to an extent that a significant unstable buoyancy gradient can be maintained in the convective layer. This is clearly seen in figure 3(b) where an unstable temperature gradient is evident in the convectively mixed layer. When the r.m.s. velocity and length scales are determined according to (1.6), the buoyancy gradient should scale as

$$\left|\left(\frac{\mathrm{d}\bar{b}}{\mathrm{d}z}\right)_{ml}\right| \sim \frac{b'}{L_r} \sim \left(\frac{q_0}{u_r}\right)\frac{1}{L_r} \sim \Omega^2, \tag{3.2}$$

and hence the ratio of buoyancy gradients in the presence and absence of rotation can be written as

$$\frac{\left|(\mathrm{d}\bar{b}/\mathrm{d}z)_{ml}\right|_{\Omega\neq 0}}{\left|(\mathrm{d}\bar{b}/\mathrm{d}z)_{ml}\right|_{\Omega=0}} \sim \left(\frac{h^2\Omega^3}{q_0}\right)^{2/3} \sim \left(\frac{h}{L_r}\right)^{4/3}. \tag{3.3}$$

Note that the parameter determining the importance of this buoyancy gradient is $R = (h^2\Omega^3/q_0)^{2/3}$, and when $h \gg L_r$, (3.3) implies that the mixed-layer buoyancy gradient in rotating convection is significant. Another interesting fact is that $(\mathrm{d}\bar{b}/\mathrm{d}z)_{ml} \sim \Omega^2$ implies that the eddies overturning in the convective layer are associated with buoyancy fluctuations of the order $\Omega^2 L_r \sim (q_0\Omega)^{1/2}$, which is in balance with the vertical inertia forces of integral-scale eddies, having an order of magnitude $w_r^2/L_r \sim (q_0/\Omega)/(q_0/\Omega^3)^{1/2} \sim (q_o\Omega)^{1/2}$. Thus, in a rotating convective turbulent layer, the vertical inertia forces are in balance with the buoyancy forces and the horizontal inertia forces are in balance with the Coriolis forces.

The presence of an interfacial buoyancy jump, or the absence thereof, has an important bearing on the growth rate of the convectively mixed layer. In studies on non-rotating convection, beginning with those of Deardorff *et al.* (1969), it has been noted that the buoyancy or the temperature jump (Δb or ΔT) at the turbulent–non-turbulent boundary (entrainment interface) is negligible (Deardorff *et al.* 1969; Fernando & Little 1990; Turner 1991), and hence it has been argued that the mixed layer grows in a non-penetrative manner so as to maintain marginal static stability at the entrainment interface ($\Delta b = \Delta T = 0$). The heat gain causes the temperature of the bottom layer to rise so as to generate an unstable temperature jump at the interface, which is immediately erased by further incorporation of fluid from above (this is also the basis for convective adjustment schemes used in numerical models). The present experiments with rotation also show that the buoyancy jump at the entrainment interface can be regarded as negligible, as exemplified by figure 3(b).

The heat balance equation can be written for the convective mixed-layer situation shown in figure 1(b) as

$$\frac{\partial \overline{T}}{\partial t} = -\frac{\partial \pi(z)}{\partial z}, \tag{3.4}$$

where $\pi(z) = -(\kappa(\partial\overline{T}/\partial z) - \overline{w'T'})$ is the total temperature flux consisting of the molecular diffusive flux $-\kappa\partial\overline{T}/\partial z$ and the turbulent temperature flux $\overline{w'T'}$. If the initial temperature profile can be written in terms of the undisturbed temperature

gradient $(\mathrm{d}\overline{T}/\mathrm{d}z)_0$ and the initial bottom temperature $\overline{T}_0$ as

$$\overline{T}(z,0) = \overline{T}_0 + \left(\frac{\mathrm{d}\overline{T}}{\mathrm{d}z}\right)_0 z, \tag{3.5}$$

then the temperature profile for $z \leqslant h$ at any time can be written in terms of h and $(\mathrm{d}\overline{T}/\mathrm{d}z)_{ml}$ as

$$\overline{T}(z,t) = \overline{T_0} + \left(\frac{\mathrm{d}\overline{T}}{\mathrm{d}z}\right)_0 h + \left(\frac{\mathrm{d}\overline{T}}{\mathrm{d}z}\right)_{ml} (z-h). \tag{3.6}$$

Note that (3.4) can be integrated with respect to z by incorporating (3.6) for $\overline{T}(z)$ when the mixed-layer buoyancy gradient $(\mathrm{d}\bar{b}/\mathrm{d}z)_{ml}$ is independent of time. This condition is satisfied in the case of (3.2) whereupon $(\mathrm{d}\bar{b}/\mathrm{d}z)_{ml}$ is fully controlled by rotation. The integrated form of (3.4) in $\int_0^h$ yields

$$\pi(0) = \left[\left(\frac{\mathrm{d}\overline{T}}{\mathrm{d}z}\right)_0 - \left(\frac{\mathrm{d}\overline{T}}{\mathrm{d}z}\right)_{ml}\right] u_e h, \tag{3.7}$$

where $\pi(0) = -\kappa\partial\overline{T}/\partial z$ is the imposed surface temperature flux, $u_e = \partial h/\partial t$ is the entrainment velocity, and the molecular diffusive flux at the top of the convective layer is neglected. Since the surface buoyancy flux q_0 is related to $\pi(0)$ as $q_0 = g\alpha\pi(0)$, (3.7) can be written in terms of the mixed-layer buoyancy gradient as

$$u_e = \frac{q_0}{[N^2 - (\mathrm{d}\bar{b}/\mathrm{d}z)_{ml}]h} \tag{3.8}$$

or

$$E = \frac{u_e}{w_\star} = \frac{1}{Ri[1 - (1/N^2)(\mathrm{d}\bar{b}/\mathrm{d}z)_{ml}]}, \tag{3.9}$$

where $Ri = N^2h^2/w_\star^2$ is the bulk Richardson number and $E = u_e/w_\star$ is the entrainment coefficient. On the other hand, if the mixed-layer buoyancy gradient is time dependent, as in the non-rotating case given by (3.1), then the entrainment coefficient needs to be adjusted accordingly. For example, when $(\mathrm{d}\bar{b}/\mathrm{d}z)_{ml} \sim (q_0/h^2)^{2/3}$,

$$E = \frac{u_e}{w_\star} = \frac{1}{Ri[1 - \frac{1}{3}(1/N^2)(\mathrm{d}\bar{b}/\mathrm{d}z)_{ml}]}, \tag{3.10}$$

and for $(\mathrm{d}\bar{b}/\mathrm{d}z)_{ml}/N^2 \ll 1$, the usual result advocated by Deardorff *et al.* (1969) and Deardorff, Willis & Stockton (1980), $E = 1/Ri$, can be recovered. Note that for non-rotating convection, the importance of the mixed-layer buoyancy gradient is determined by the parameter $(q_0/h^2N^3)^{2/3}$ whereas in rotationally dominated mixed layers the parameter $S = \Omega^2/N^2$ determines the significance of the mixed-layer buoyancy gradient in the entrainment process. As discussed before, the mixed-layer buoyancy gradient is expected to be affected by rotation above a critical value of $R = (h^2\Omega^3/q_0)^{2/3}$.

4. Results

4.1. *Qualitative observations*

Observations made by injecting fluorescent dye into the mixed layer clearly showed that the dye is distributed rapidly throughout the mixed layer for the non-rotating case and occurs at a slower pace for the rotating case. The latter observation can

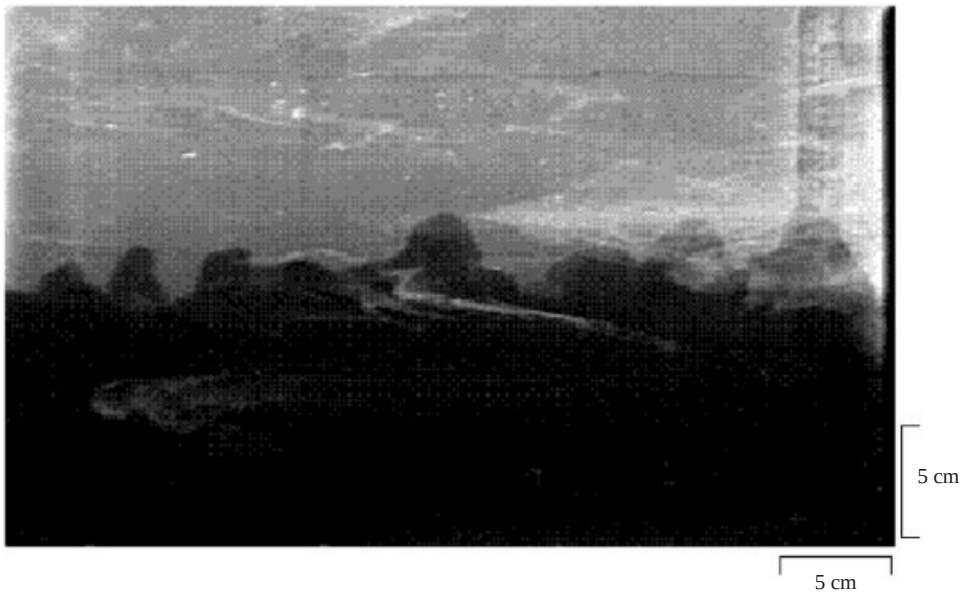

FIGURE 5. Video image of the entrainment zone, as identified by colouring the bottom convective layer with dye. Note the hummocks created by the impingement of eddies on the entrainment interface. $N = 0.3\,\mathrm{rad\,s^{-1}}$, $q_0 = 0.01\,\mathrm{cm^2\,s^{-3}}$, $\Omega = 0\,\mathrm{rad\,s^{-1}}$ (non-rotating case).

be attributed to the formation of isolated vortices near the heating surface, which retard the horizontal dispersion, and the Taylor column effect in the vertical direction which slows the vertical movement and facilitates the development of a vertical destabilizing buoyancy gradient. In this case, the turbulence in the convective layer is scaled as in (1.6), very different from its non-rotating counterpart (1.3). In the non-rotating case, plume-like fluid elements that developed near the bottom boundary ascended intermittently, and some of them impinged on the entrainment interface that separates the turbulently convecting and top stratified layers. These buoyant fluid elements penetrated partially into the outer stratified layer, creating dome-like protrusions at the interface; see figure 5. These puffy domes have some resemblance to fair weather cumulus clouds sometimes found on top of the atmospheric convective boundary layer. As plumes penetrate into the stratified layer, they are subjected to a negative buoyancy force, and hence rebound back into the convecting layer. During the penetration process, thin layers of fluid sandwiched between the stratified layer and the puffs can be 'squeezed' downward into the mixed layer. These fluid elements can be broken down by the surrounding turbulence, and the disintegrated fluid parcels so produced are incorporated into the mixed layer while completing the entrainment process. However, close inspection of interfacial events and entrainment data reveal that this penetrative entrainment mechanism, involving the squeezing out of lighter fluid by the buoyant plumes forcing against the stratified layer, is of lesser importance than the encroachment mechanism driven by the static instability at the interface; the latter causes layers of unstable fluid at the interface to tumble down into the mixed layer, which, in turn, homogenized with the convective turbulent layer. The rate limiting step appears to be the encroachment rate (the measurements to be discussed in § 4.3 show that the entrainment-rate estimates based on encroachment agree well with the experimental data).

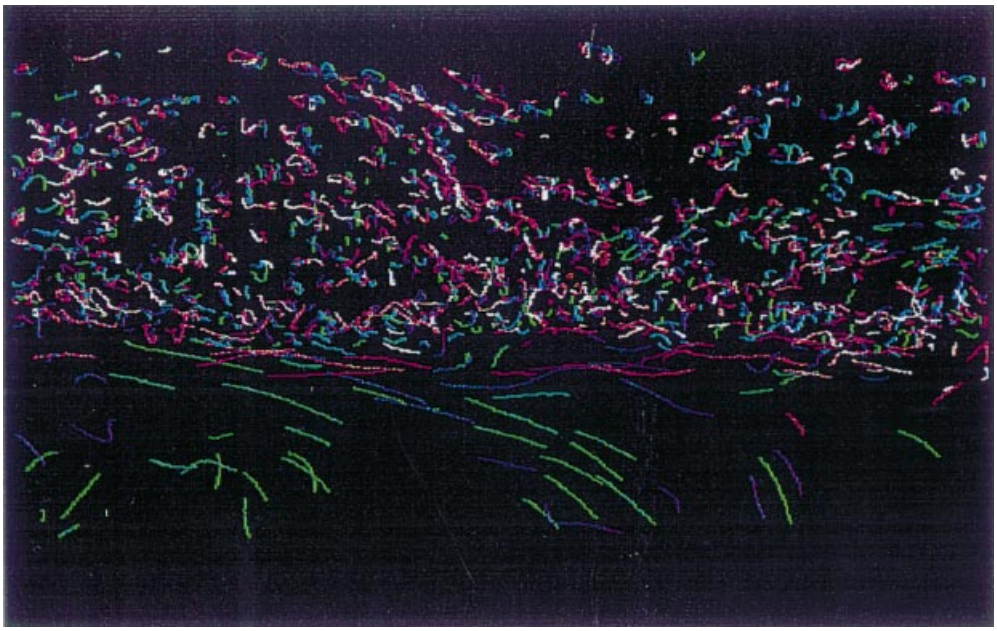

FIGURE 6. A close-up view of the interface (a 10 cm wide section), as identified by the motion of neutrally buoyant particles suspended in the flow. The bottom layer is turbulent and the top layer is temperature stratified. Note the presence of weaker internal-wave motions (indicated by closed pathlines) in the top layer, induced by the disturbances created by eddies impinging on the interface. The particle paths are traced for 60 s. The colour-coded intensity (0–255 levels) was changed by 8 units every 3 s in order to locate a particle at a specific time during tracking.

Observations made with suspended particles in the upper stratified layer clearly showed the existence of 'circular' pathlines, indicating the presence of internal waves in the stratified layer, arguably excited by plumes impinging on the interface (figure 6). Since the entrainment is driven by static instability at the interface, and hence the energy content of turbulent eddies is of secondary importance for entrainment, these internal waves are expected to have insignificant influence on the entrainment rate. These waves, however, can have an influence on the vertical transport of heat in the stratified layer through advective–diffusive processes. What is important here is the ability of eddies to mix the heat flux over the convective layer at a rate faster than the rate at which the encroachment of buoyant fluid from the upper layer can occur. The agreement of entrainment rate measurements with those predicted based on encroachment mechanisms suggests that this is true for both non-rotating (Deardorff *et al.* 1969) and rotating (§ 4.3) cases. Also note that the entrainment rate in the rotating case is smaller, and hence, though the turbulence is rotationally affected, can sustain mixing of encroached fluid.

Figure 7(a, b) shows photographs of the convective layer taken in the presence of rotation. A marked difference can be seen between key features of figures 5 and 7(a) in that the interface of the latter consists of finger-like (lenticular) plumes of horizontal scales much smaller than those observed for the non-rotating case. Careful observations indicate that these plumes are the apexes of cyclonic vortices that originate near the heated surface, at the base of the convective layer; apparently, they concentrate the background 'planetary' vorticity to produce strong cyclonic vorticity within rising plumes. Figure 7(b) shows the evolution of dye introduced near the

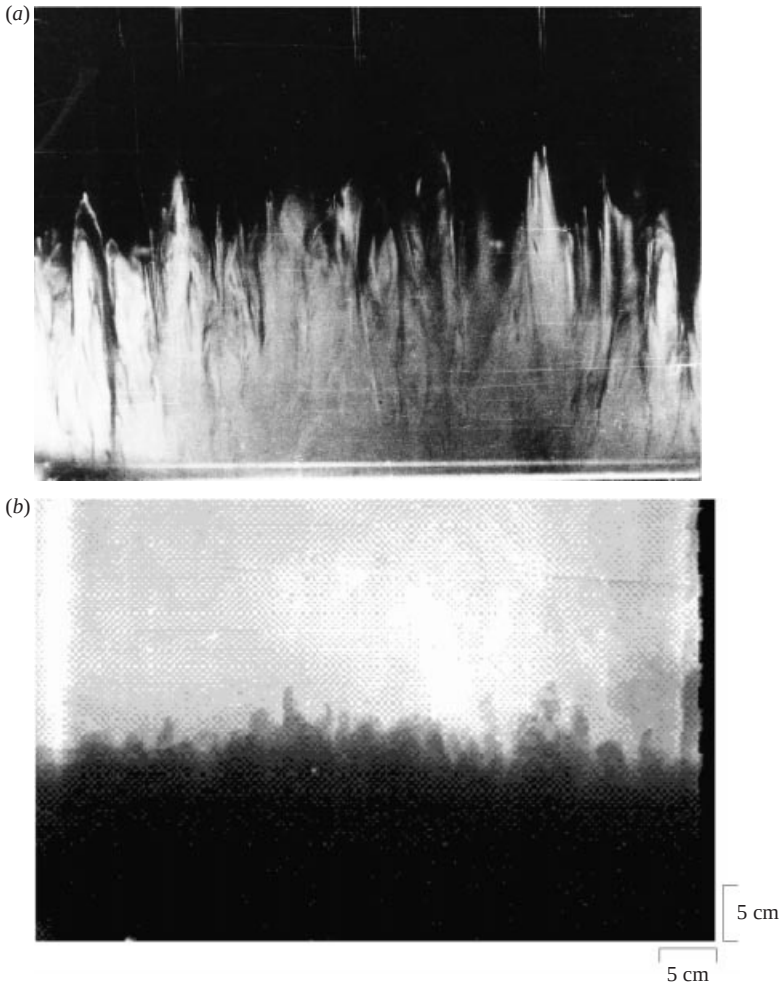

FIGURE 7. Views of the entrainment interface in rotating convection. Note the lenticular vortices generated at the bottom, and extending past the interface. These vortices move laterally, sometimes interacting with each other. (*a*) $q_0 = 0.014\,\mathrm{cm^2\,s^{-3}}$, $\Omega = 0.94\,\mathrm{rad\,s^{-1}}$. (*b*) $q_0 = 0.02\,\mathrm{cm^2\,s^{-3}}$, $\Omega = 0.5\,\mathrm{rad\,s^{-1}}$, $(h^2\Omega^3/q_0)^{2/3} = 100$. The non-uniform dye distribution in (*a*) is due to the insufficient time allowed to mix the dye in the convective layer. Almost the entire width of the tank is in view.

bottom heated surface, illustrating the presence of vortices. Note that the fluorescent dye in figures 5 and 7(*a*, *b*) was added during the growth phase of the convective layer for visualization purposes, and the photos do not indicate the long-term distribution of dye. For example, at large times, dye in figure 7(*a*) is distributed uniformly in the bulk of the convective layer showing lenticular undulations in the interfacial area characteristic of figure 7(*b*). The generation of such intense isolated vortices in rotating turbulent convection has been reported for the laboratory experiments of Chen *et al.* (1989) and Brickman & Kelley (1993). In the present case, these vortices appear to have a noticeable effect on the interfacial motion field, yet the influence of these motions on the rate of entrainment is minimal, as the experimental data presented in § 4.3 indicate.

The formation of intense vortices during rotating turbulent convection in rotating

stratified fluids has also been reported from the direct numerical simulation studies of Julien *et al.* (1996, 1999) and large-eddy simulations of Fernando & Smith (2001). Julien *et al.* (1996) found that these vortices are key to the lateral stirring of the boundary layer near the buoyancy source, leading to high rates of turbulent kinetic energy dissipation. Their work also indicated the formation of finger-like undulations at the entrainment interface due to the influence of these vortices. Although these vortices alter the stirring patterns in the convective layer, the growth of the convective layer is governed by the non-penetrative encroachment mechanism as described above, and hence the nature of the vortices plays a secondary role in the convective layer growth. The conical appearance of the vortices has some similarities with those expected during fluid parcel motion at or near the marginal stability of rotating convection (Veronis 1959). As pointed out by Boubnov & Golitsyn (1995), however, such structures are effaced at higher supercriticalities due to the plume structures generated by turbulence.

4.2. *Measurement of the buoyancy gradients*

During the experiments, the buoyancy gradient along each probe traverse was evaluated, and a number of profiles (> 20) obtained using the three probes were averaged to evaluate the average buoyancy gradient in the convective layer. As evident from figure 3(b), the buoyancy gradient is negative for this case. On dimensional grounds, it is possible to expect that the buoyancy gradient in the convective mixed layer in the presence of rotation is given by

$$\left(\frac{\mathrm{d}\bar{b}}{\mathrm{d}z}\right)_{ml} = f_1(q_0, \Omega, h), \tag{4.1}$$

or

$$\frac{(\mathrm{d}\bar{b}/\mathrm{d}z)_{ml}}{\Omega^2} = f_2(R), \tag{4.2}$$

where f_1, and f_2 are functions. The large amount of buoyancy gradient data was broken up into a number of bins, such that $[\log(R_{upper\ limit}) - \log(R_{lower\ limit})] = 0.2$. Then, all the data falling within a particular bin were averaged to produce a single data point. Based on (4.2), the averaged data were then plotted on a $B = |(\mathrm{d}\bar{b}/\mathrm{d}z)_{ml}|/\Omega^2$ versus $R = (h^2\Omega^3/q_0)^{2/3}$ graph, which is shown in figure 8. The largest R used corresponded to the experiments with no initial stratification. The data show a decreasing trend in the range $R < R_c$, where $R_c \approx 275$, according to

$$f_2 \sim R^{-1}, \tag{4.3}$$

indicating that

$$\left|\left(\frac{\mathrm{d}\bar{b}}{\mathrm{d}z}\right)_{ml}\right| \sim \left(\frac{q_0}{h^2}\right)^{2/3}, \tag{4.4}$$

close to what is expected in non-rotating fluids according to (3.1). This indicates that the buoyancy gradient in the convective layer is not dynamically affected by the rotation when $R < R_c$. However, when $R > R_c$, the buoyancy gradient follows the asymptotic scaling law

$$\frac{\left|(\mathrm{d}\bar{b}/\mathrm{d}z)_{ml}\right|}{\Omega^2} = C, \tag{4.5}$$

where $C \approx 0.02 \pm 0.005$, much the same as what is expected from (3.2). The critical value R_c was selected based on the intersection of (4.3) and (4.5) and has an uncertainty of $\pm 20\%$.

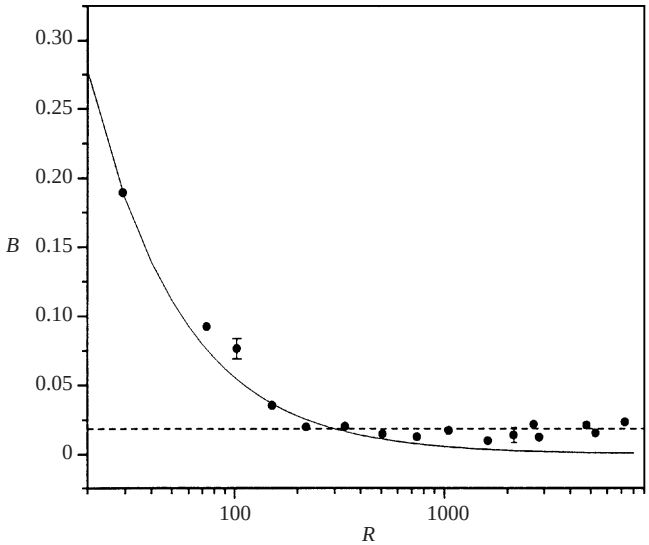

FIGURE 8. Normalized mean mixed-layer buoyancy gradient $B = (\mathrm{d}\bar{b}/\mathrm{d}z)_{ml}/\Omega^2$ as a function of $R = (h^2\Omega^3/q_0)^{2/3}$, bin averaged. The error bars represent one standard deviation from the average value shown. The solid line shows the $f_2 \sim R^{-1}$ behaviour of (4.3) obtained using scaling arguments. The data points at large R (> 3000) are from experiments carried out in homogeneous fluids.

The above finding of the departure of buoyancy scaling from (4.4) is consistent with the findings of Coates & Ivey (1997) who conducted velocity measurements in rotating convection. They observed that the velocity scaling of rotating convection deviated from non-rotating scaling (1.6) when the inverse Rossby number Ro^{-1} becomes approximately 20 (more precisely, when Ro^{-1} increases from 10 to 20). Here the Rossby number is defined as $Ro = (q_0/f^3h^2)^{1/3}$, where $f = 2\Omega$, and hence $Ro = 1/(2R^{1/2})$. Our observations indicate that this transition may occur between $R_c \approx 150$ and $R_c \approx 200$, or $Ro^{-1} \approx 25$–28, which is consistent with Coates & Ivey's (1997) results. The critical $R_c \approx 275$ ($Ro^{-1} \approx 33$) proposed here, however, was derived by assuming an abrupt transition between the two regimes, based on curve fitting to the regimes according to (4.3) and (4.5).

4.3. *The growth of the convective mixed layer*

The average mixed-layer height h at a given time t was used to evaluate the rate of entrainment during the experiments (§ 2), and a typical h versus t graph is shown in figure 9. Also shown in this figure is a curve depicting $h = \beta t^n$, where β and n are constants for a given experiment provided that the data are taken in the same (rotationally affected) regime. Here, the time $t = t^\star - t_0$ is measured from a virtual origin t_0 determined by a graph of the form $h = \beta(t^\star - t_0)^n$, where $t^\star$ is the time measured from the onset of heating. Best fits to all the runs for depths greater than 8 cm yielded an approximately constant t_0 when $n \approx 0.5$ was selected; see figure 9. Although the data were collected covering $3 < h < 30$ cm, only those for $h > 8$ cm were used for the curve fits to ensure that all data belong to the same rotationally dominated regime. Note that β can be evaluated by assuming that the encroachment mechanism described in § 2 is valid for this case and that the entrainment law is given by (3.9). Substitution of (4.5) into (3.8) gives

$$h^2 = \frac{2q_0}{(N^2 + C\Omega^2)}t, \quad R > R_c, \tag{4.6}$$

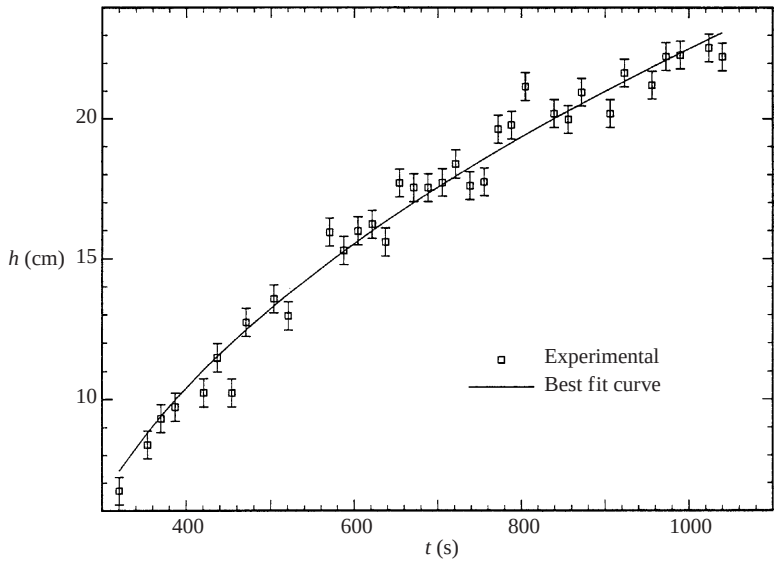

FIGURE 9. The square symbols represent mixed-layer height measurements from successive profiles during an experiment. The line is a curve of the form $h = \beta t^{1/2}$ used to calculate the entrainment velocity.

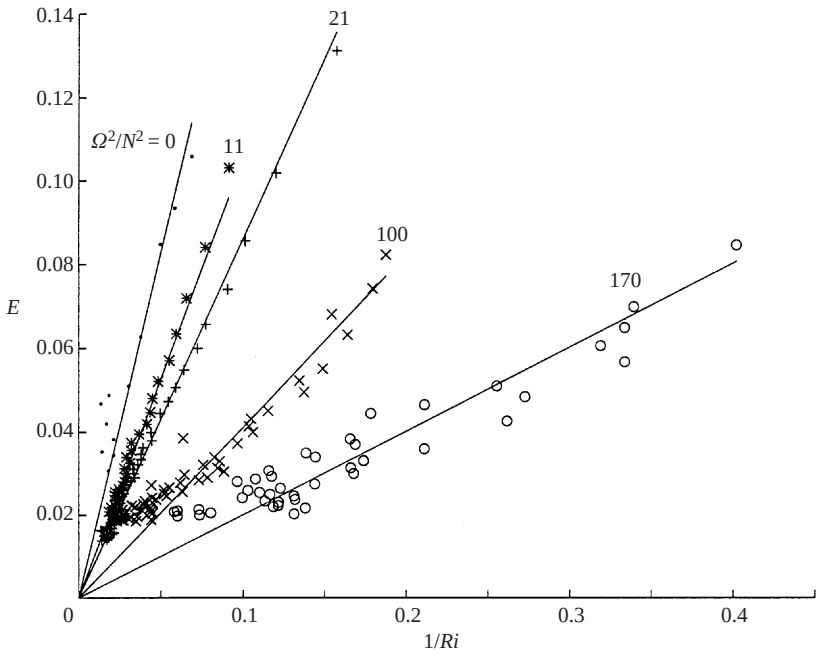

FIGURE 10. A plot of entrainment coefficient E versus the inverse Richardson number Ri^{-1} for rotating convection experiments carried out with different values of Ω^2/N^2, including $\Omega^2/N^2 = 0$.

based on which $\beta = \sqrt{2q_0/(N^2 + C\Omega^2)}$. Also, (3.9) simply becomes

$$E = \frac{1}{Ri(1 + C\Omega^2/N^2)}. \tag{4.7}$$

Figure 10 shows plots of E versus $1/Ri$ for sets of experiments carried out at $R > R_c$,

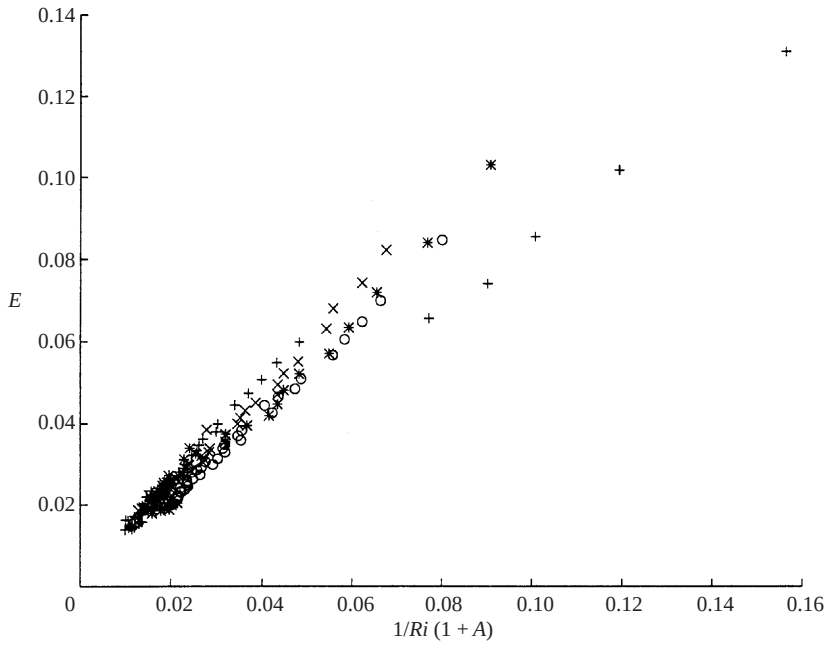

FIGURE 11. A plot of entrainment coefficient versus $[Ri(1+A)]^{-1}$ where $A = 0.02\Omega^2/N^2$, for experiments shown in figure 10.

wherein the background rotation plays a dominant role in developing the mixed-layer buoyancy gradient. Also shown are the data from an experiment where $R = 0$. It is clear that the entrainment rate in the presence of rotation is significantly smaller than its non-rotating counterpart that obeys the entrainment law $E \approx 1/Ri$. These data are rearranged and are plotted in figure 11 as a plot of E versus $1/Ri(1 + C\Omega^2/N^2)$, with $C \approx 0.02$, concurrent with (4.7). The data collapse well, indicating strong support for (4.7).

Julien *et al.* (1996) presented entrainment results based on numerical experiments. They examined the inverse problem of cooling a rotating stably stratified fluid from above for three different rates of rotation; $\Omega = 0$, 0.074 and $0.23\,\mathrm{rad\,s^{-1}}$. Their experimental runs are in the range $0 \leqslant R \leqslant 17.9$ and hence convective-layer growth should not be significantly affected by the background rotation. This is consistent with their observation that the mixed-layer buoyancy gradient at different rates of rotation is not much different from the non-rotating case. In addition, the largest value of Ω^2/N^2 used in their study was 0.155 and hence the effect of the $C\Omega^2/N^2$ term is negligibly small. The present work shows that Ω^2/N^2 must equal at least about 5 before the entrainment laws begin to significantly deviate from the inverse Richardson number law (figure 10). This is also in agreement with the Julien *et al.* (1996) data that indicate that the rate of entrainment is only slightly affected by rotation in the parameter range used. Nevertheless, they found the formation of lenticular vortices at the cooling surface, which extend into the convective layer as was discussed in § 4.1. The images of the interface presented in their paper also show the formation and protrusion of lenticular vortices into the underlying stratified layer, as was observed in our experiments.

5. Conclusions and discussion

An experimental study dealing with the growth of a turbulent convective layer in a linearly stratified fluid was described in the foregoing sections. The flow configuration consisted of a heat-stratified fluid of buoyancy frequency N, subjected to uniform bottom heating with a buoyancy flux q_0 in the presence of background rotation of rotational frequency Ω. During the evolution of the fluid system, the mixed-layer depth h grows with time t, and the effects of stratification and rotation on the growth rate were studied. Some non-rotating experiments were also carried out, with which the rotating experiments could be compared. The results show that:

(i) Convection in both rotating and non-rotating experiments occurs in a non-penetrative manner, whereby no appreciable buoyancy jump develops at the entrainment interface during the mixed-layer growth. However, a dynamically significant unstable buoyancy gradient develops within the convective layer in the presence of rotation. In the case of non-rotating convection or in rotating convection satisfying $(h^2\Omega^3/q_0)^{2/3} < R_c$, with $R_c \approx 275$, the buoyancy gradient in the convective layer satisfies the relation

$$\left|\left(\frac{\mathrm{d}\bar{b}}{\mathrm{d}z}\right)_{ml}\right|_{\Omega=0} \approx 5.5\left(\frac{q_0}{h^2}\right)^{2/3}, \tag{5.1}$$

whereas for $(h^2\Omega^3/q_0)^{2/3} > R_c$ the buoyancy gradient satisfies

$$\left|\left(\frac{\mathrm{d}\bar{b}}{\mathrm{d}z}\right)_{ml}\right|_{\Omega\neq0} \approx 0.02\Omega^2. \tag{5.2}$$

The ratio between the two cases is $|(\mathrm{d}\bar{b}/\mathrm{d}z)_{ml}|_{\Omega\neq0}/|(\mathrm{d}\bar{b}/\mathrm{d}z)_{ml}|_{\Omega=0} \gg 1$. This result is of practical utility in convective adjustment schemes that are used to parameterize convection in geophysical mixed-layer models. In such schemes, if an unstable buoyancy gradient develops in the turbulent layer, the fluid region is instantaneously overturned computationally so as to erase this density gradient. Our results imply that this procedure should be used with caution in the presence of background rotation, as significant unstable gradients can be sustained within the turbulent layer when $R > R_c$. Constraints imposed by rotation on vertical motions (an extreme case is the Taylor–Proudman limit) are responsible for the sustenance of such unstable gradients in rotating turbulent convection.

(ii) Although the convection is non-penetrative, detailed flow visualization studies on the non-rotating case show that the entrainment interface is perturbed and penetrated by turbulent eddies, which excite internal waves in the stratified layer. In the rotating case, too, the inertial–gravity waves can be excited, but the interfacial distortions take the form of finger-like intrusions driven by intermittently appearing vortices in the convective layer. This is consistent with the large-eddy simulation of deep convection by Garwood (1998) which show significant leakage of turbulent kinetic energy past the mixed-layer base.

(iii) Based on the notion of non-penetrative convection, expressions were proposed for the rate of growth of the convective mixed layer u_e for non-rotating and rotating cases, which were in good agreement with the data. In particular, when $(h^2\Omega^3/q_0)^{2/3} < R_c$, the entrainment law is

$$\frac{u_e}{w_\star} \approx \frac{1}{Ri}, \tag{5.3}$$

whereas for $(h^2\Omega^3/q_0)^{2/3} > R_c$,

$$\frac{u_e}{w_\star} \approx \frac{1}{Ri(1 + 0.02\Omega^2/N^2)}. \tag{5.4}$$

In the following, the application of the present results to natural deep convective situations is discussed. Typical oceanic values are $q_0 = 10^{-7}\,\mathrm{m^2\,s^{-3}}$, $h \sim 1\,\mathrm{km}$ and $\Omega \sim 5 \times 10^{-5}\,\mathrm{rad\,s^{-1}}$, and hence $(h^2\Omega^3/q_0)^{2/3} \approx 1.16$, indicating that Earth's rotational effects can be considered as unimportant in determining oceanic deep convective-layer growth. (During deep convection, nonetheless, the convective layer can be embedded with lenticular vortices formed due to rotational effects). Thus, one-dimensional mixed-layer models of the form $E \sim Ri^{-1}$ should be applicable to oceans prior to the onset of two- and three-dimensional effects due to baroclinic instabilities. A similar assertion can be made for atmospheric deep convection where $\Omega \sim 7 \times 10^{-5}\,\mathrm{rad\,s^{-1}}$, $h \sim 10\,\mathrm{km}$, and $q_0 \sim 10^{-5}\,\mathrm{m^2\,s^{-3}}$, which gives $(h^2\Omega^3/q_0)^{2/3} \sim O(1)$.

Measurements of buoyancy gradients in oceanic deep convective layers are sparse, but most of the available data indicate that within the convective layer the buoyancy gradients are negligible (Schott & Leaman 1991). This is consistent with the present work that indicates negligible buoyancy gradients when $R < 275$. It should be born in mind, however, that the ocean's convective layers include many other phenomena such as horizontal advection, spatial and temporal non-uniformity of the buoyancy flux and non-uniform stratification. Hence, the application of laboratory results to oceanic convection should be done with caution.

Schott, Visbeck & Send (1994) have reported measurements of mixed-layer deepening during the Greenland Sea oceanic deep convection. These were made during the winter of 1988–1989, in a period where the Greenland Sea deep water formation was weak, sporadic, and associated with cold air outbursts. The heat flux during this period was highly variable, varying from 40 to $7500\,\mathrm{W\,m^{-1}}$. In February, a mixed-layer deepening event was detected due to increased convective activity, with typical mixed-layer depth of $h \sim 250\,\mathrm{m}$, buoyancy flux $q_0 \sim 10^{-8}\,\mathrm{m^2\,s^{-3}}$ and background $N \sim 10^{-4}\,\mathrm{rad\,s^{-1}}$. Given that $(h^2\Omega^3/q_0)^{2/3} \sim 0.85$, based on $\Omega \sim 5 \times 10^{-5}\,\mathrm{rad\,s^{-1}}$, the mixed-layer buoyancy gradients are not expected to be affected by the background rotation. Thus the entrainment rate u_e can be calculated using (5.3) and $Ri \approx 3.4$ as $u_e \approx 0.4\,\mathrm{cm\,s^{-1}}$. This is in reasonable agreement with the observation reported by Schott *et al.* (1994), $u_e \approx 0.3\,\mathrm{cm\,s^{-1}}$. On the other hand, measurements during March 6–16 indicated that the deep convection has penetrated to 2000 m or so and the convective layer has a well-defined negative buoyancy gradient. Arguably, the buoyancy flux during this period has been low, of the order of $10^{-9}\,\mathrm{m^2\,s^{-3}}$, and hence $(h^2\Omega^3/q_0)^{2/3} \sim 62$. Although this value of R is smaller than $R_c \approx 275$, observation of the development of a buoyancy gradient at larger R is encouraging. A similar observation has also been noted during Labrador Sea measurements (Lazier, Rhines & Lilly 1998).

Elongated vortices that cause perturbations at the interface have been observed in oceans; for example, see the observations reported by Schott & Leaman (1991) in the Gulf of Lyons. Significant spatial undulations at the mixed-layer base have also been reported by D'Asaro *et al.* (1996) during the Labrador Sea deep convection experiment, based on the tracks of neutrally buoyant floats deployed in the convective layer (also see the numerical results of Fernando & Smith 2001). In addition, both the Greenland Sea deep convection observations of Schott *et al.* (1994) and the Gulf of Lyons' observations of Leaman & Schott (1991) indicate that, during the mixed-layer deepening, the density jump at the entrainment zone is negligible, implying

non-penetrative convection. This observation is also in agreement with that reported here.

The authors wish to thank Rui-rong Chen and Greg Cole for their assistance in numerous ways and Dr C. Y. Ching for his endless technical support. The funding for this work was primarily provided by the Office of Naval Research, High Latitude Programs. Stratified and Rotating flow research at Arizona State University is also supported by the National Science Foundation and the Army Research Office.

REFERENCES

Adrian, R. J., Ferreira, R. T. D. S. & Boberg, T. 1986 Turbulent thermal convection in wide horizontal fluid layers. *Exps. Fluids* **4**, 121–141.

Boubnov, B. M. & Golitsyn, G. S. 1995 *Convection in Rotating Fluids*. Kluwer.

Brickman, D. & Kelley, D. E. 1993 Development of convection in a rotating fluid: Scales and patterns of motion. *Dyn. Atmos. Oceans* **19**, 389–405.

Castaing, B., Gunaratne, G., Heslot, F., Kadanoff, L., Libchaber, A., Thomae, S., Wu, X., Zaleski, S. & Zanetti, G. 1989 Scaling of hard thermal turbulence in Rayleigh–Bénard convection. *J. Fluid Mech.* **204**, 1–30.

Chen, R., Fernando, H. J. S. & Boyer, D. L. 1989 Formation of isolated vortices in a rotating convecting fluid. *J. Geophys. Res.* **94**, 18445–18453.

Coates, M. J. & Ivey, G. N. 1997 On convective turbulence and the influence of rotation. *Dyn. Atmos. Oceans* **25**, 217–232.

Colomer, J., Zieren, L. D. & Fernando, H. J. S. 1998 Comments on the Paper 'Localized Convection in Rotating Stratified Fluid'. *J. Geophys. Res.* **103**, 12891–12894.

D'Asaro, E., Farmer, D. M., Osse, J. T. & Daiviki, G. T. 1996 A Lagrangian float. *J. Atmos. Oceanic Tech.* **13**, 1230–1246.

Deardorff, J. W. 1972 Numerical investigation of neutral and unstable planetary boundary layers. *J. Atmos. Sci.* **29**, 91–115.

Deardorff, J. W. & Willis, G. E. 1985 Further results form a laboratory model of the convective planetary boundary later. *Boundary Layer Met.* **32**, 205–236.

Deardorff, J. W., Willis, G. E. & Lilly, D. K. 1969 Laboratory investigation of nonsteady penetrative convection. *J. Fluid Mech.* **35**, 7–31.

Deardorff, J. W., Willis, G. E. & Stockton, B. H. 1980 Laboratory studies of entrainment zone of a convective mixed layer. *J. Fluid Mech.* **100**, 41–62.

Fernando, H. J. S., Chen, R. & Boyer, D. L. 1991 Effects of rotation on convective turbulence. *J. Fluid Mech.* **228**, 513–547.

Fernando, H. J. S. & Little, L. J. 1990 Molecular-diffusive effects in penetrative convection. *Phys. Fluids* **2**, 1592–1596.

Fernando, H. J. S. & Smith, D. C. IV 2001 Vortex structures in turbulent convection. *Eur. J. Mech./*B *Fluids* **20**, 437–471.

Fleury, M., Mory, M., Hopfinger, E. J. & Auchere, D. 1991 Effects of rotation on turbulent mixing across a density interface. *J. Fluid Mech.* **223**, 165–191.

Garwood, R. W. Jr. 1998 Large-eddy simulation of Labrador Sea winter convection, Part 1: Turbulent kinetic energy (TKE) and salinity variations. Presented at the Ocean Sciences Meeting of the American Geophysical Union. *EOS* **79**, 184.

Greenspan, H. 1980 *The Theory of Rotating Fluids*. Cambridge University Press.

Ivey, G. N., Taylor, J. R. & Coates, M. J. 1995 Convectively driven mixed layer growth in a rotating, stratified fluid. *Deep-Sea Res.* **42**, 331–349.

Jones, H. & Marshall, J. 1993 Convection with rotation in a neutral ocean: A study of open-ocean deep convection. *J. Phys. Oceanogr.* **23**, 1009–1039.

Julien, K., Legg, S., McWilliams, J. & Werne, J. 1996 Penetrative convection in rapidly rotating flows: Preliminary results from numerical simulations. *Dyn. Atmos. Oceans* **24**, 227–236.

Julien, K., Legg, S., McWilliams, J. & Werne, J. 1999 Plumes in rotating convection. Part 1. Ensemble statistics and dynamical balances. *J. Fluid Mech.* **391**, 151–187.

Kaimal, J. C., Wyngaard, J. C., Haugen, D. A., Cote, O. R., Izumi, Y., Caughey, S. J. & Reading, C. J. 1976 Turbulence structure in the convective boundary layer. *J. Atmos. Sci.* **33**, 39–46.

Krishnamurty, R. 1970 On the transition to turbulent convection. Part 2. The transition to turbulent time-dependent flow. *J. Fluid Mech.* **42**, 295–302.

Lazier, J. R., Rhines, P. B. & Lilly, J. 1998 Is deep convection penetrative? A tentative analysis of density-time series. Presented at the Ocean Sciences Meeting of the American Geophysical Union. *EOS* **79**, 184.

Leaman, K. D. & Schott, F. 1991 Hydrographic structure of the convection regime in the Gulf of Lyons: Winter 1987. *J. Phys. Oceanogr.* **21**, 575–598.

Levy, M. A. 1998 Turbulent thermal convection in a rotating stratified fluid. MS Thesis, Arizona State University.

Marshall, J. & Schott, F. 1998 Open-ocean convection: Observations, theory and models. *Rep* 52, Center for Global Change Science, Massachusetts Institute of Technology.

Molemaker, M. J. & Dijkstra, H. A. 1997 The formation and evolution of a diffusive interface. *J. Fluid Mech.* **331**, 199–229.

Schott, F. & Leaman, K. D. 1991 Observations with moored acoustic Doppler current profilers in the convection regime in the Golfe du Lion. *J. Phys. Oceanogr.* **21**, 558–574.

Schott, F., Visbeck, M. & Send, U. 1994 Open ocean deep convection, Mediterranean and Greenland seas. In *Ocean Processes in Climate Dynamics: Global and Mediterranean Examples*, pp. 203–225. Kluwer.

Siggia, E. D. 1994 High Rayleigh number convection. *Annu. Rev. Fluid. Mech.* **26**, 137–168.

Sullivan, P., Moeng, C.-H., Stevens, B., Lenschow, D. H. & Mayor, S. D. 1998 Structure of the entrainment zone capping the convective atmospheric boundary layer. *J. Atmos. Sci.* **55**, 3042–3064.

Turner, J. S. 1973 *Buoyancy Effects in Fluids*. Cambridge University Press.

Turner, J. S. 1991 Convection and mixing in the oceans and the Earth. *Phys. Fluids* A **3**, 1218–1232.

Veronis, G. 1959 Cellular convection with finite amplitude in a rotating fluid. *J. Fluid Mech.* **5**, 401–435.

Voropayev, S. I. & Fernando, H. J. S. 1999 Evolution of two-layer thermohaline systems under surface cooling. *J. Fluid Mech.* **380**, 117–140.

Whitehead, J. A., Marshall, J. & Hufford, G. E. 1996 Localized convection in rotating stratified fluid. *J. Geophys. Res.* **101**, 25705–25721.

Willis, G. E. & Deardorff, J. W. 1974 A laboratory model of the unstable planetary boundary layer. *J. Atmos. Sci.* **31**, 1297–1307.